The parent body controls on cosmic spherule texture: Evidence from the oxygen isotopic compositions of large micrometeorites

M. Van Ginneken, J. Gattacceca, P. Rochette, Corinne Sonzogni, Anne
Alexandre, Vladimir Vidal, M. J. Genge

The parent body controls on cosmic spherule texture: Evidence from the oxygen isotopic compositions of large micrometeorites

M. van Ginneken [a,b,*], J. Gattacceca [c], P. Rochette [c], C. Sonzogni [c], A. Alexandre [c], V. Vidal [c], M.J. Genge [a]

[a] *IARC, Department of Earth Science and Engineering, Imperial College London, Exhibition Road, London SW7 2AZ, UK*
[b] *Department of Earth Sciences, The Natural History Museum, Cromwell Road, London SW7 5BD, UK*
[c] *CNRS/Aix-Marseille Université, IRD, Collège de France, CEREGE UM34, Aix-en-Provence, France*

Abstract

High-precision oxygen isotopic compositions of eighteen large cosmic spherules (>500 μm diameter) from the Atacama Desert, Chile, were determined using IR-laser fluorination – Isotope Ratio Mass spectrometry. The four discrete isotopic groups defined in a previous study on cosmic spherules from the Transantarctic Mountains (Suavet et al., 2010) were identified, confirming their global distribution. Approximately 50% of the studied cosmic spherules are related to carbonaceous chondrites, 38% to ordinary chondrites and 12% to unknown parent bodies. Approximately 90% of barred olivine (BO) cosmic spherules show oxygen isotopic compositions suggesting they are related to carbonaceous chondrites. Similarly, ~90% porphyritic olivine (Po) cosmic spherules are related to ordinary chondrites and none can be unambiguously related to carbonaceous chondrites. Other textures are related to all potential parent bodies. The data suggests that the textures of cosmic spherules are mainly controlled by the nature of the precursor rather than by the atmospheric entry parameters. We propose that the Po texture may essentially be formed from a coarse-grained precursor having an ordinary chondritic mineralogy and chemistry. Coarse-grained precursors related to carbonaceous chondrites (i.e. chondrules) are likely to either survive atmospheric entry heating or form V-type cosmic spherules. Due to the limited number of submicron nucleation sites after total melting, ordinary chondrite-related coarse-grained precursors that suffer higher peak temperatures will preferentially form cryptocrystalline (Cc) textures instead of BO textures. Conversely, the BO textures would be mostly related to the fine-grained matrices of carbonaceous chondrites due to the wide range of melting temperatures of their constituent mineral phases, allowing the preservation of submicron nucleation sites. Independently of the nature of the precursors, increasing peak temperatures form glassy textures.
© 2017 The Authors. Published by Elsevier Ltd. This is an open access article under the CC BY license (http://creativecommons.org/licenses/by/4.0/).

Keywords: Micrometeorites; Cosmic spherules; Oxygen isotopes; Laser fluorination; Parent bodies

1. INTRODUCTION

Micrometeorites are extraterrestrial particles 10 μm–2 mm in size, which represent in terms of mass the most important part of the flux of extraterrestrial material to accrete to the Earth's surface (Rubin and Grossman, 2010). One of the most important objectives of studies on micrometeorites is to identify their parent bodies. Studies based on petrographic and mineralogical evidence have suggested that between 75% and 99% of unmelted micrometeorites ≤250 μm in size should have fine-grained precursors similar to the matrices of carbonaceous chondrites (Engrand and Maurette, 1998; Noguchi et al., 2002; Taylor et al., 2012).

The measurement of the triple isotopic composition of oxygen is a powerful tool for the classification of planetary materials and allows correlation with known parent bodies in the solar system (Clayton et al., 1991; Clayton and Mayeda, 1999). A clear distinction, for example, between ordinary chondrites and carbonaceous chondrites is possible because, on a $\delta^{17}O/\delta^{18}O$ chart, the former plots above the terrestrial fractionation line (hereafter TFL and defined by $\delta^{17}O = 0.52 * \delta^{18}O$), whereas, except for the CI chondrites that overlap the TFL, the latter plots below the TFL. Studies based on ion microprobe analyses have shown that the oxygen isotopic bulk compositions of micrometeorites mostly plot below the TFL, therefore suggesting that these particles have carbonaceous chondrite-related precursors (Clayton and Mayeda, 1999; Engrand et al., 2005; Taylor et al., 2005; Yada et al., 2005). However, the large analytical uncertainties of ion microprobe analyses (± 1–2.75‰ on $\delta^{18}O$, ± 0.7–1.7‰ on $\delta^{17}O$, and ± 0.6–1.7‰ on $\Delta^{17}O$ for individual analyses; Engrand et al., 2005; Yada et al., 2005) mean that values close to the compositional field of ordinary chondrites ($\Delta^{17}O \approx 0.5$–1.5‰) overlap with the TFL, preventing a clear identification of the parent bodies of these micrometeorites. Recent studies aiming at determining the oxygen isotopic composition of melted micrometeorites from the Transantarctic Mountains (TAM) > 500 μm in size, have used the IR-laser fluorination – Isotope Ratio Mass spectrometry (IRMS) technique (Cordier et al., 2011a; Suavet et al., 2010, 2011; Cordier and Folco, 2014). An advantage of this technique is its high reproducibility and accuracy which allow a clear identification of micrometeorites having oxygen isotopic compositions plotting close to the TFL (e.g., ordinary chondrite-related precursors). An important conclusion from these studies is that in the size fractions studied, the contribution of micrometeorites having ordinary chondrite-related precursors is significant (i.e., between 30% and 70%).

Suavet et al. (2010) noted that micrometeorites plot in four discrete groups on a three-oxygen diagram, each linked to distinct parent bodies. In particular, the discovery of micrometeorites having oxygen isotopic compositions that are not linked to any known parent body showed that micrometeorites include samples of small solar system objects not sampled by meteorites.

The main aim of this study is to further identify the parent bodies of cosmic spherules using high resolution oxygen isotopes by IR-laser fluorination-IRMS and thus to examine whether the textural types of cosmic spherules relate to parent body or are imposed by the nature of melting in the atmosphere as suggested by Suavet et al. (2010) on a much smaller dataset. If texture could be used as a proxy for parent body then the contribution of different sources to the Earth's extraterrestrial dust flux could be evaluated using data from thousands of characterized particles rather from just a limited number of particles for which oxygen isotope data is available. Cosmic spherules (CS, i.e. fully melted micrometeorites) from the Atacama Desert are used in this study since they not only include large enough particles (i.e. >500 μm) to perform IR-laser fluorination-IRMS but also provide a useful comparison to the previously analyzed TAM collection particles that will allow study of the distribution of the parent bodies of CSs.

2. MATERIALS AND METHODS

2.1. Samples

Cosmic spherules were randomly extracted from soil collected in 2006 in the Atacama Desert (Chile) at 24.43°S, 70.31°W following a methodology developed in Antarctica (Rochette et al., 2008). Hutzler et al. (2016) have shown that this area yields a meteorite density of the order of 100 meteorite >10 g/km² and exposure ages >5 Ma. This explains the high density of micrometeorites in the sampled soil. Soil was first sieved (200–800 μm), and then submitted to magnetic separation. Micrometeorites were then hand-picked from the magnetic fraction under a binocular microscope, on the basis of their spherical shape and dark color. This technique yielded over 2000 magnetic CSs, lacking the non-magnetic V-type CSs, which mainly consist of glass (Genge et al., 2008). The present study focuses on 18 CSs >500 μm in size. Their masses range from 235 to 627 μg (530–820 μm in diameter, respectively). Prior to analyses of the triple isotopic composition of oxygen, CSs showing obvious effects of terrestrial weathering under SEM (e.g., silicate crystal dissolution; Van Ginneken et al., 2016) were treated with HCl in order to remove possible alteration products, such as carbonates and sulfates, which may affect the primary isotopic signature of the particles. Several non-destructive techniques were used to characterize these CSs before the oxygen isotope measurements. In addition to 14 particles already collected and studied by Kohout et al. (2014), four CSs, #10.16, #10.17, #10.18 and #10.20, were selected at CEREGE (Aix-en-Provence, France) for oxygen isotope analyses (Fig. 1).

2.2. Characterization methods

2.2.1. Petrography

Information on the external structure of these four particles was gathered using a LEO 1455 environmental
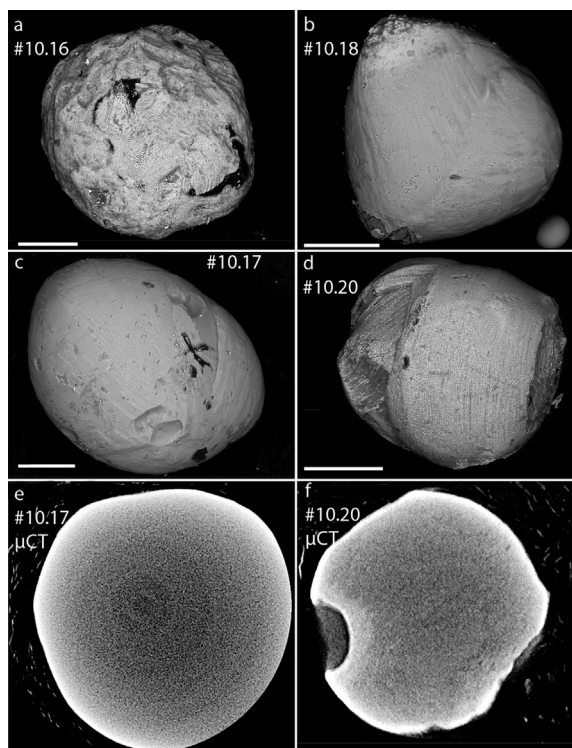
Fig. 1. Scanning electron microscope backscattered electron images of four cosmic spherules (a) #10.16 (cryptocrystalline), (b) #10.18 (cryptocrystalline), (c) #10.17 (cryptocrystalline) and (d) #10.20 (barred olivine). The scalebars are 100 μm. (e and f) μCT sections of #10.17 and #10.20. The external structure of cryptocrystalline CS #10.17 (c) shows olivine crystals ~1 μm in size that are not observed in the μCT section (e). In contrast, the external structure of #10.20 (d), which is typical of barred olivine CSs, is also faintly observed in μCT sections (f).

scanning electron microscope (SEM) at the Imaging and Analysis Centre (IAC) of the National History Museum (NHM) London.

2.2.2. X-ray computed microtomography

The internal structure of the CSs was determined using X-ray computed microtomography (μCT). The experimental procedure for 14 particles is available in Kohout et al. (2014). The internal structure of the remaining four CSs (i.e. #10.16, #10.17, #10.18 and #10.20) was studied using a Xradia MicroXCT-400 at CEREGE. A tungsten source was used, with running conditions of 140 kV and 70μA. The voxel size (vs) in the final 3D rendering is dependent on both a geometric magnification (i.e. distance of the sample from both the X-ray source (ds) and the detector (dd)) and an optical magnification of x20 applied in front of the detector. These two parameters were manually controlled for each samples (#10.16: ds (in mm) = 42.8, dd (in mm) = 33.5, vs (in μm) = 0.75; #10.17: ds = 47.3, dd = 28.0, vs = 0.84; #10.18: ds = 41.8, dd = 33.5, vs = 0.74; #10.20: ds = 41.8, dd = 33.5, vs = 0.74. For each particles, 2501 images were acquired, with an exposure time of 20 s each. Finally, the resulting data was processed using the Avizo software.

2.2.3. Magnetic measurements

A magnetic characterization of the selected CSs was performed prior to the oxygen isotope measurements. Hysteresis parameters — saturation magnetization M_S, saturation remanent magnetization M_{rs} and coercivity B_c — were measured at CEREGE with a Princeton Measurements Corporation Vibrating Sample Magnetometer (VSM) (noise level of $\sim 10^{-9}$ A m^2). The remnant coercive field B_{cr} was determined by DC backfield demagnetization of the saturation remnant magnetization using the VSM.

2.2.4. Oxygen isotope measurements

Measurements of $\delta^{18}O$ and $\delta^{17}O$ of the CSs were carried out at the Stable Isotopes Laboratory of CEREGE, using the laser-fluorination-IRMS technique (Alexandre et al., 2006; Crespin et al., 2008) adapted for the measurement of extraterrestrial materials (Suavet et al., 2010). The triple isotopic composition was measured with a dual-inlet mass spectrometer Thermo-Finnigan Delta Plus. The gas (O$_2$) was passed through a -114 °C slush to condense potential interfering gasses before being sent to the mass spectrometer. In order to get sufficient 34/32 and 33/32 signals (2–3 V), the oxygen from standards and CSs was concentrated in the mass spectrometer in an auto-cooled 800 μl microvolume filled with silica gel and directly connected to the dual-inlet system.

The oxygen isotope results are expressed in ‰ versus V-SMOW. Measured $\delta^{18}O$ and $\delta^{17}O$ values of the samples were corrected on a daily basis using a ~ 1.5 mg quartz laboratory standard "Boulangé" (Alexandre et al., 2006; Suavet et al., 2010). During the analyzing period, a calibration of the reference gas was made. Replicate analysis of NBS-28 ($\delta^{18}O = 9.60 \pm 0.12‰$; $\delta^{17}O = 4.99 \pm 0.08‰$; $\Delta^{17}O = 0.00 \pm 0.03‰$; $n = 19$) and Boulangé ($\delta^{18}O = 16.25 \pm 0.16‰$; $\delta^{17}O = 8.44 \pm 0.09‰$; $\Delta^{17}O = -0.01 \pm 0.03$; $n = 31‰$) were carried out.

Measurements made on microsamples (<400 μg) of Boulangé using the mass spectrometer-cooled microvolume showed a systematic offset from the larger samples values for $\delta^{18}O$, $\delta^{17}O$ and $\Delta^{17}O$ ($-0.96 \pm 0.30‰$ for $\delta^{18}O$, $-0.69 \pm 0.14‰$ for $\delta^{17}O$, $-0.19 \pm 0.07‰$ for $\Delta^{17}O$, $n = 9$), which is very close to the offset measured in Suavet et al., 2010, ($\Delta^{17}O = -0.16 \pm 0.05‰$). Correction for these offsets were applied on $\delta^{18}O$ and $\delta^{17}O$ for small mass samples (<400 μg).

3. RESULTS

3.1. Classification of the cosmic spherules

The physical properties of 14 particles were determined by Kohout et al. (2014) using μCT and X-ray diffraction (XRD) to allow the entire mass to be used for oxygen isotope analysis without preserving material for petrologic study. The particles were subsequently classified as cryptocrystalline (Cc) and glass (V-type) CSs (Genge et al., 2008). Distinction between V-type CSs (i.e. composed essentially of glass) and Cc CSs is not possible using μCT alone, due to the minimum voxel size that is larger than the size of olivine crystals constituting Cc CSs (e.g., Fig. 1e;

Table 1
Oxygen isotopic compositions and magnetic properties of cosmic spherules from the Atacama Desert.

Sample	Texture	Group[a]	Mass (μg)	Diameter (μm)	$\delta^{18}O$[b]	$\delta^{17}O$[b]	$\Delta^{17}O$[b]	M_s	Magnetite[c]	B_{cr}/B_c	M_{rs}/M_s
9.1	Cc	3	326	630	17.6	9.6	0.4	3.96	4.31	1.66	0.44
9.2	BO	1	235	530	27.3	11.1	−3.1	8.09	8.80	2.33	0.13
9.3	BO	3	489	850	15.8	8.8	0.6	4.95	5.38	1.56	0.47
9.9	BO	2	254	550	21.9	10.6	−0.8	5.80	6.31	1.50	0.34
10.2	BO	2	254	610	23.4	10.8	−1.4	2.79	3.03	n.d.	0.57
10.3	BO	1	353	670	24.7	9.6	−3.2	8.31	9.04	2.50	0.11
10.6	BO	3	310	710	21.5	11.8	0.6	9.63	10.47	1.85	0.29
10.8	BO	1	265	630	34.3	15.6	−2.2	15.7	17.2	2.60	0.11
10.9	BO	1	338	680	32.8	14.3	−2.8	10.1	11.0	2.22	0.13
10.10	Cc	3	247	550	16.9	9.4	0.6	3.73	4.05	1.53	0.33
10.11	Cc	4	292	670	31.4	17.2	0.8	7.45	8.09	1.85	0.17
10.12	Cc	1	300	600	31.3	11.8	−4.4	5.01	5.45	1.95	0.23
10.13	Cc	4	405[d]	700	42.6	23.5	1.4	1.95	2.12	2.00	0.15
10.14	BO	1	266	630	16.7	4.2	−4.4	5.13	5.57	1.62	0.18
10.16	BO	1	450[d]	710	20.0	6.2	−4.3	4.89	5.31	2.16	0.17
10.17	Cc	3	627[d]	820	20.5	10.6	0.0	2.17	2.36	1.48	0.52
10.18	Cc	3	280	570	13.8	7.5	0.3	5.04	5.47	1.76	0.22
10.20	BO	2	245	500	23.1	10.9	−1.1	1.49	1.62	1.80	0.38

n.d. = not determined
Textures: Cc = cryptocrystalline; BO = barred olivine.
[a] As defined in the text.
[b] in ‰ vs V-SMOW.
[c] Magnetite content in wt.%.
[d] Correction of offset from the larger samples values for $\delta^{18}O$, $\delta^{17}O$ and $\Delta^{17}O$ was applied for samples <0.4 mg.

Genge et al., 2008). In contrast, the degree of crystallinity determined using XRD allow a clear distinction between the highly crystalline Cc CSs and the amorphous V-type CSs. On the basis of XRD data available in Kohout et al. (2014), V-type particles are here reclassified as Cc CSs. The whole selection studied here consists of 11 barred olivine (BO) and 7 Cc CSs (Genge et al., 2008).

The magnetic properties of the particles are consistent with previous studies of CSs from the TAM (Table 1; Suavet et al., 2009, 2010, 2011). Magnetite is the main magnetic mineral in CSs with occasional Fe-Ni droplets (Suavet et al., 2009). The saturation magnetization is, thus, directly proportional to the amount of magnetite in the CSs (pure magnetite wt.% = Ms/0.92; Dunlop, 2002). In the present study, the magnetite content ranges from 1.6 to 17.2 wt. %, which is similar to the magnetite content in CSs from the TAM (e.g., Suavet et al., 2011). The M_{rs}/M_s ratio is related to the domain state of magnetite grains, and is inversely proportional to the size of the grains (Day, 1977). Results are broadly consistent with those from the literature (Suavet et al., 2010, 2011), with Cc CSs having pseudosingle domain to single domain grains and BO CSs having larger grains in the pseudo-single domain range.

3.2. Oxygen isotopic composition

The $\delta^{18}O$, $\delta^{17}O$ and $\Delta^{17}O$ values for the micrometeorites are reported in Table 1. In Fig. 2, the data is shown compared to the terrestrial fractionation line (TFL), the carbonaceous chondrite anhydrous mineral (CCAM) line, and to the oxygen isotopic compositions of micrometeorites from other works (Cordier et al., 2011a, 2012; Engrand

et al., 2005; Taylor et al., 2005; Yada et al., 2005; Suavet et al., 2010, 2011) and meteorites (Clayton et al., 1991; Clayton and Mayeda, 1999; Newton and Pillinger, 2000). The isotopic compositions of the CSs were grouped according to the four groups defined qualitatively by Suavet et al. (2010) (Fig. 3). Seven BO CSs have isotopic compositions in the Group 1 (below the TFL with $\Delta^{17}O \approx -4.4‰$ to $-2.2‰$ and $\delta^{18}O \approx 16-34‰$). Three BO CSs have isotopic compositions in the Group 2 (below the TFL, with $\Delta^{17}O \approx -1.4‰$ to $-0.8‰$ and $\delta^{18}O \approx 22‰$). Four Cc and two BO CSs have isotopic compositions in the Group 3 (above the TFL, with $\Delta^{17}O \approx 0.04-0.6‰$ and $\delta^{18}O \approx 13-21‰$). The two Cc CSs #10.11 and #10.13 have isotopic compositions in the ^{16}O-poor Group 4 (above the TFL, with $\Delta^{17}O \approx 0.8‰$ and $1.4‰$, and $\delta^{18}O \approx 31-43‰$, respectively).

4. DISCUSSION

4.1. Parent bodies of micrometeorites

Due to significant melting during atmospheric entry heating, the primary mineralogy, chemistry and isotopic composition of CSs have been significantly modified (Alexander et al., 2002; Taylor et al., 2005; Yada et al., 2005; Genge et al., 2008). The oxygen isotopic signature of the CSs is controlled by several factors: the isotopic composition of their precursor material, fractionation processes occurring during their entry in the Earth's atmosphere, and incorporation of atmospheric oxygen. During atmospheric entry, CSs are flash-melted at high altitude (∼80 km), before being quenched in a few seconds (Love and Brownlee, 1991). Flash-heating experiments using meteorite
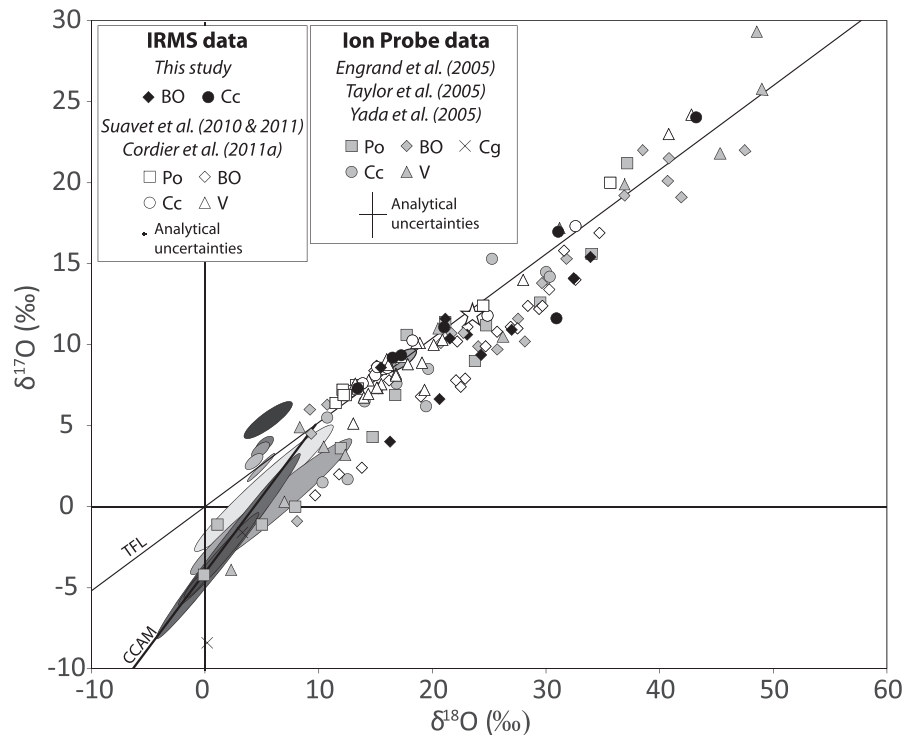
Fig. 2. Oxygen isotopic compositions of cosmic spherules (in ‰ vs. V-SMOW) from the Atacama Desert and from Antarctica (using IRMS in Cordier et al., 2011a; Suavet et al., 2010, 2011; and ion probe in Engrand et al., 2005; Taylor et al., 2005; Yada et al., 2005). Typical 2σ analytical uncertainties for the two analytical techniques are represented. Compositional fields for carbonaceous, ordinary, rumuruti and enstatite chondrites are represented (Clayton et al., 1991; Clayton and Mayeda, 1999; Newton and Pillinger, 2000). The solid line labeled TFL is the terrestrial fractionation line (approximated $\delta^{17}O = 0.52 \times \delta^{18}O$), and the solid line labeled CCAM is the carbonaceous chondrite anhydrous minerals line (approximated $\delta^{17}O = 0.938 \times \delta^{18}O - 4.06$) (Clayton and Mayeda, 1999).

samples have shown that exchange between meteoritic oxygen and gaseous oxygen is possible in less than a minute (Yu et al., 1995). During the formation of CSs, such mixing will cause their precursor's isotopic composition to evolve toward that of tropospheric oxygen, which plots slightly below the TFL (Fig. 3; $\delta^{18}O \approx 23.5‰$, $\delta^{17}O \approx 11.8‰$; Thiemens et al., 1995). As a result of this mixing, CSs spherules having ordinary chondrite parentage will have lower value of $\Delta^{17}O$, and vice versa for CSs having carbonaceous chondrite parentage. Another process affecting the isotopic composition of CSs is a mass-dependent fractionation due to evaporation occurring during atmospheric entry (Yada et al., 2005; Suavet et al., 2010). Evaporation occurs during melting of the particles and affects the chemical and isotopic composition of the CSs to various extents depending on the peak temperature (Alexander et al., 2002). This mass-dependent fractionation will deplete the particle in the lighter ^{16}O, therefore shifting their original isotopic signature toward higher $\delta^{18}O$ and $\delta^{17}O$ values, on a line parallel to the TFL on a $\delta^{17}O$ vs $\delta^{18}O$ diagram (Fig. 3).

The isotopic compositions of the CSs from the Atacama Desert are shown in Fig. 3, compared to other high-precision oxygen isotope compositions of micrometeorites acquired using the IRMS technique (Cordier et al., 2011a; Suavet et al., 2010, 2011). Isotopic compositional fields of chondritic meteorites based on whole-rock analyses are also displayed (Clayton et al., 1991; Clayton and Mayeda, 1999;

Newton and Pillinger, 2000). Oxygen isotopic compositions of CSs determined using ion microprobe (Engrand et al., 2005; Taylor et al., 2005; Yada et al., 2005) were not used due to the large uncertainties associated with this technique ($\approx \pm 1.2‰$ for $\delta^{18}O$ and $\approx \pm 1‰$ for $\Delta^{17}O$, against $\pm 0.3‰$ for $\delta^{18}O$ and $\pm 0.2‰$ for $\Delta^{17}O$ for IRMS data). These large uncertainties prevent a clear identification of the parent bodies having affinities with the ordinary chondrite, for which $\Delta^{17}O$ varies between 0.5‰ and 1.5‰. The mixing with atmospheric oxygen and the mass-dependent fraction due to evaporation described above have also been modeled in Fig. 3, by taking ordinary chondrites and carbonaceous chondrites as starting material. The shaded areas represent the range of oxygen isotopic compositions of CSs having ordinary chondrite-related (light gray area) or carbonaceous chondrite-related (dark gray area) parent bodies.

Whole-rock oxygen isotope analyses of chondritic material (Clayton et al., 1991; Clayton and Mayeda, 1999; Newton and Pillinger, 2000) were favored over analyses of individual phases that have been the subject of recent studies (Chaussidon et al., 2008; Libourel and Chaussidon, 2011; Rudraswami et al., 2011; Tenner et al., 2013, 2015; Wakaki et al., 2013; Weisberg et al., 2011). These studies focused on components of carbonaceous chondrites exhibiting extreme oxygen isotopic signatures plotting outside the compositional fields defined using whole-rock analyses (e.g., spinels in CAIs extremely
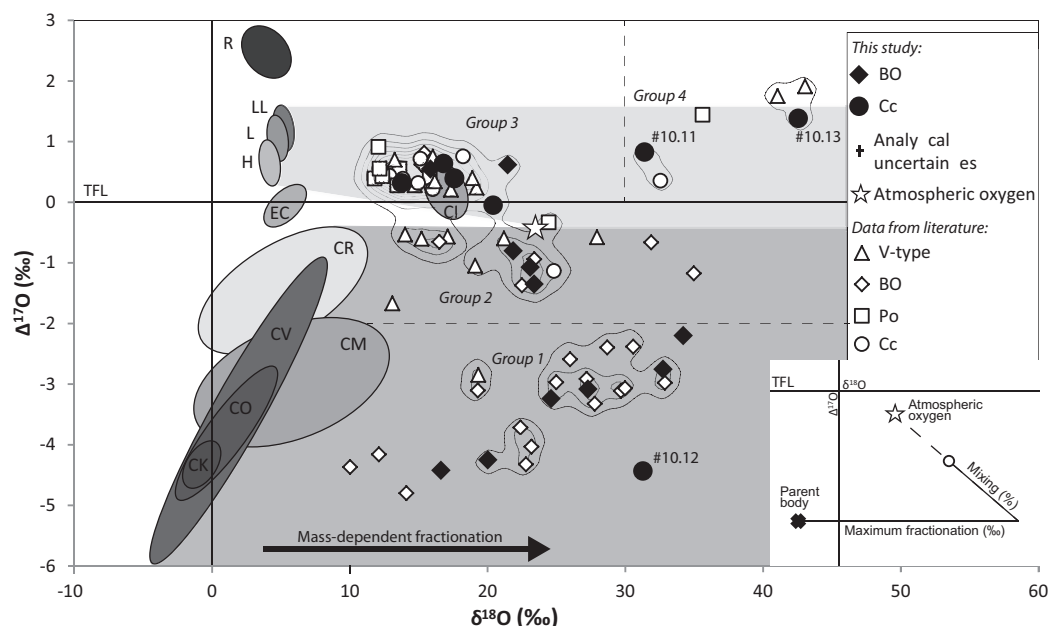
Fig. 3. $\Delta^{17}O$ vs. $\delta^{18}O$ values (in ‰ vs. V-SMOW) of individual cosmic spherules from the Atacama Desert and from the Transantarctic Mountains measured by IRMS (Cordier et al., 2011a; Suavet et al., 2010, 2011). Analytical uncertainties (2σ) are represented. Density contours are shown. Compositional fields of the potential parent bodies are displayed (Clayton et al., 1991; Clayton and Mayeda, 1999; Newton and Pillinger, 2000). The range of possible values of $\Delta^{17}O$ and $\delta^{18}O$ for a micrometeorite from carbonaceous (dark gray) and ordinary (light gray) chondrites are represented by shaded areas. The four isotopic groups were first defined by Suavet et al. (2010). Particles in group 1 have $\delta^{18}O$ values ranging from ~10‰ to ~35‰ and $\Delta^{17}O$ values ≤2‰; particles in group 2 have similar $\delta^{18}O$ values and $\Delta^{17}O$ values ≥2‰; particles in group 3 have $\delta^{18}O$ values ranging from ~10‰ and ~20‰ and $\Delta^{17}O$ values ≤1‰; particles in group 4 have $\delta^{18}O > 30‰$ and $\Delta^{17}O$ ranging between 0‰ and 1.8‰. Dashed lines represent roughly isotopic group boundaries.

enriched in ^{16}O or carbonates in CM chondrites exhibiting $\Delta^{17}O > 0$). These extreme oxygen isotopes values may shift the isotopic signatures of the precursors of CSs toward values outside of compositional fields determined using whole-rock analyses. However, modal abundances of carbonates and CAIs in carbonaceous chondrites are usually low (≪5 vol.%), their sizes limited (≤100 μm) and their distribution sparse (Endreβ and Bischoff, 1996; Hezel et al., 2008; Howard et al., 2009; King et al., 2015; De Leuw et al., 2010). Components of chondrules exhibiting extreme oxygen isotope signatures are also limited in size (few tens of micrometers; Chaussidon et al., 2008; Libourel and Chaussidon, 2011; Rudraswami et al., 2011; Tenner et al., 2013, 2015). Assuming that the precursors of CSs are likely to be 1.5–2 times larger than the resulting spherules (i.e. >750 μm for the large CSs studied here; Love and Brownlee, 1991), we suggest that such components exhibiting extreme isotopic signatures will only account for less than 1 vol.% of the whole particles. Therefore, such extreme isotopic signatures are unlikely to have significant impacts on the bulk oxygen isotopic signature of complex assemblages of minerals that are the precursors of large CSs. Therefore, we suggest that whole-rock oxygen isotope analyses of chondrites are better proxies to the isotopic signatures of the precursors, and thus parent bodies, of large CSs. Note that this may not be the case for CSs from smaller size fractions, as suggested by extremely ^{16}O-rich isotopic signatures of small CSs (i.e. <200 μm in size) determined using Ion Probe (Yada et al., 2005).

Fig. 3 shows that isotopic signatures of CSs from the Atacama Desert plot in the same discrete groups defined for CSs from the Transantarctic Mountains (Suavet et al., 2010). Based on the compilation from the four successive studies (Fig. 3) we may define more quantitatively the limit between the four groups: $\Delta^{17}O < -2$, $-2 < \Delta^{17}O < -0.5$, $0 < \Delta^{17}O < 1$ and $1.5 < \Delta^{17}O$ for groups 1–4, respectively. This suggests that terrestrial weathering effects, which may potentially affect the oxygen isotope signature of extraterrestrial material collected on the Earth's surface (e.g., Bland et al., 2006), are negligible, as expected after selection of externally unweathered samples and precautionary removal of potential terrestrial weathering products by HCl treatment on particles from both collections (Suavet et al., 2010).

In the present study nine BO CSs and one Cc CS (~55% of studied samples) plotting in Group 1 and Group 2 are likely to be related to carbonaceous chondrites. It is noteworthy that no particle exhibit $\Delta^{17}O$ above ~0.3‰, therefore excluding enstatite chondrites (EC) as potential parent material (i.e. minimum $\Delta^{17}O$ values of EC is 0.297‰). The three particles having $\Delta^{17}O = <-4‰$ cannot be related to CM and CR chondrites only, because these two chondrite classes display $\Delta^{17}O$ values >−4‰. These CSs are likely related to CV, CO or CK parent bodies. Suavet et al. (2010) argued that the maximum amount of mass-dependent fractionation and the percentage of mixing with atmospheric oxygen are related to the atmospheric entry parameters of the CSs (i.e., velocity and entry angle);

in order to have coherent entry parameters between particles of Group 1 and Group 2, these authors suggested that particles in the former must be related to CV-CO-CK chondrites only, whereas particles in the latter must be related to CM-CR chondrites. The Cc CS #10.12 has a $\delta^{18}O$ that is at least 10‰ higher than BO CSs having similar $\Delta^{17}O$ (Fig. 3). This may be explained by increased mass dependent fractionation that is directly related to increased evaporation due to higher peak temperatures during atmospheric entry. Determining the exact shift in $\delta^{18}O$ as a function of evaporation is not possible though. However, Alexander et al. (2002) have shown that CSs that suffered the strongest peak temperatures also show the strongest increase in $\delta^{18}O$ values. Since Cc CSs are thought to have suffered higher peak temperatures than BO CSs (e.g., Taylor et al., 1998), it is reasonable to assume that the shift toward higher $\delta^{18}O$ has been more important for particle #10.12 compared to BO CSs having similar $\Delta^{17}O$.

As explained above, mixing with atmospheric oxygen will tend to shift the $\Delta^{17}O$ of CSs toward that of the tropospheric oxygen, which plot slightly below the TFL. Therefore, CSs having parent bodies lying above the TFL (e.g., Group 3) could potentially have negative $\Delta^{17}O$ values, between that of the TFL and of tropospheric oxygen, if mixing with atmospheric oxygen was almost complete. On the other hand, it is not possible for CSs having carbonaceous chondrite-related parent bodies (i.e., Groups 1 and 2) to have an isotopic signature above the TFL. As a consequence, although having absolute $\delta^{18}O$ values similar to those of particles in Group 2, the 4 Cc CSs and 2 BO CSs (~33% of studied samples) plotting in Group 3 are likely to have ordinary chondrite-related parent bodies. It is noteworthy that the Cc CS #10.17 has a $\Delta^{17}O$ value of approximately 0.0‰, therefore, an EC parent body is possible. Other particles in Group 3 have $\Delta^{17}O$ values that are not consistent with EC material though. Furthermore, cosmic spherules #10.17, along with #10.6, have $\delta^{18}O$ values ~3‰ higher than the maximum $\delta^{18}O$ of CI chondrites, while having $\Delta^{17}O$ consistent with both ordinary chondrites and CI chondrites. As a result, based on $\Delta^{17}O$ values, a CI chondrite parent body for these CSs cannot be ruled out. Previous works have pointed out that all CSs in groups 1 and 2, the shift toward higher $\delta^{18}O$ values due to mass-dependent fractionation ranges between 10‰ and ~40‰ (Suavet et al., 2010, 2011; Cordier et al., 2012). A minimum shift of ~10‰ is also observed for the BO and Cc CSs of the group 3 that are only related to ordinary chondrites (i.e., CSs having $\delta^{18}O$ values lower than CI chondrites). The mineralogy and textures of these spherules are identical, therefore, it is safe to assume that they have suffered the same minimum amount of fractionation. Thus, we suggest that a OC parentage for CSs exhibiting a shift ≪10‰ from the maximum $\delta^{18}O$ value of CI chondrites but similar $\Delta^{17}O$ is more likely, even if CI parentage cannot be excluded entirely. As mentioned above, particle Cc CS #10.17 can potentially have OC or EC parent bodies, in equal measure.

The two Cc CSs #10.11 and #10.13 plot in a ^{16}O-poor area of the three-oxygen diagram (Fig. 3), defined in previous works focusing on large CSs as the group 4 (Suavet

et al., 2010, 2011). Note that such ^{16}O-poor CSs have been observed in smaller size fractions as well (Yada et al., 2005). An ordinary chondrite-related parent body for #10.11 would require an extreme mass-dependent fractionation (> 30‰). This seems unlikely, as other Cc CSs that are related to ordinary chondrites show a maximum fractionation of ~20‰. Similarly, a CI chondrite-related parent body for #10.11 can be ruled out, as it would imply significant fractionation and negligible mixing with atmospheric oxygen, as its $\Delta^{17}O$ is equal to the maximum $\Delta^{17}O$ value for CI chondrites. A Rumuruti chondrite-related parent body cannot be excluded for #10.11 and #10.13, although this would also require extreme mass-dependent fractionation (> 30‰). Considering only isotopic signatures, other potential parent bodies for these two particles include magnetites and mesostasis in unequilibrated chondrites (Choi et al., 1998; Franchi et al., 1999). Suavet et al. (2010) also argued that two V-type CSs in group 4 having isotopic signatures almost identical to #10.13 (shown in Fig. 3) may be related with the ^{17}O-rich end member of the cristobalite line trend (Bridges et al., 1998). However, these potential precursor materials cannot explain the mineralogy of the resulting Cc CSs. Another possible parent material is the new-poorly characterized phase (new-PCP) observed in the ungrouped carbonaceous chondrite Acfer 094 (Sakamoto et al., 2007). This mineral phase, composed essentially of Fe, Ni, O and S, exhibit particularly high $\delta^{18}O$ and $\delta^{17}O$ values (~180‰). Such oxygen signature would require extreme mixing with atmospheric oxygen and/or with other primitive components exhibiting lower $\delta^{18}O$ and $\delta^{17}O$ values (e.g. matrix). Although this cannot be ruled out, similar extreme mixing with atmospheric oxygen are not observed in S-type CSs and the relatively small size of known new-PCP (<10 μm) suggest that they cannot efficiently shift the bulk isotopic signature of a precursor of large CSs toward values consistent with CSs in Group 4. Finally, another probable possibility is that #10.11 and #10.13 sample one of several yet unknown parent bodies, having chondritic chemical compositions and mineralogy, but distinct isotopic composition, similarly to what is proposed for CSs of smaller sizes (Yada et al., 2005).

A striking result of this work is that on a selection of 18 randomly selected CSs from the Atacama Desert collection, there are members of all four discrete isotopic groups defined by 58 CSs from the TAM collection (Suavet et al., 2010, 2011; Cordier et al., 2012). Interestingly, apart for particle #10.12 outlying group 1, the range of $\delta^{18}O$ and $\Delta^{17}O$ values are broadly identical for CSs from both collections, suggesting that both collections are representative of the mean flux of CSs to Earth.

The fact that CSs having isotopic signatures in the group 4 are also observed in the Atacama Desert collection suggests that this group's parent bodies, although not represented by meteorites, contribute significantly to the flux of extraterrestrial matter to Earth. The present study confirms that the distribution of CSs observed in previous studies on particles from the TAM that are located more than 8500 km from the Atacama Desert, is global and unaffected by biases related to abnormal local events or removal by weathering. Considering the very different environments

of Antarctica and the Atacama desert, the fact that weathering does not produce a significant bias emphasizes that cosmic spherule collections can be broadly representative as long as S-types survive.

We confirm in this study of CSs >500 μm in size, the significant part of OC related parentage (OC proportion of 33% and 39% for the Atacama Desert and TAM collections, respectively), at odds with previous results on micrometeorites <250 μm (e.g., Engrand and Maurette, 1998). We can propose different explanations for this dichotomy:

- In ion probe studies the near TFL data has not been interpreted in terms of parent bodies; due to uncertainties some part of this population may be OC related.
- Studies of small micrometeorites have often focused on unmelted particles; the hydrated mineralogy and high porosity of CC-derived micrometeorites may result in a large thermal gradients that will prevent their core from melting (Genge, 2006).
- There is a genuine dependence of the OC/CC ratio versus particle size in interplanetary space, due to the larger friability of CC versus OC that results in the overproduction of CC-derived particles <300 μm in size (Flynn et al., 2009).
- A more recent study on unmelted micrometeorites has shown that in the 50–300 μm size range, ~70% of the coarse-grained particles are related to OC, representing ~18% over the total populations of MMs (Genge, 2008). Further high-precision oxygen isotope studies on CSs in smaller size ranges should help at better identifying their parent bodies.

4.2. Relation between texture and parent body

Table 2 shows the relative abundance of parent bodies within CSs from the TAM and Atacama Desert collections. Eighty-six percent of BO CSs from the TAM and Atacama collections analyzed for oxygen isotopes appear to be related to carbonaceous chondrites and the remainder to ordinary chondrites (Fig. 3 and Table 2). Accordingly, 75% of carbonaceous chondrite-related CSs exhibit the BO texture. In contrast ~89% of the Po CSs appear related to ordinary chondrites, with the exception of one that is related to an unknown parent body (i.e. Group 4; Fig. 3). None of the Po CSs are related to carbonaceous chondrites as noted previously (Suavet et al., 2010, 2011). Similarly, 67% of Cc CSs are related to ordinary chondrites and only 13% to carbonaceous chondrites. V-type CSs are related to all types of parent bodies. This study, therefore, confirms that texture provides a means to identify a likely parent body without the need for oxygen isotope analysis (Suavet et al., 2011), however, the origin of the parent body control on texture is important in evaluating the degree of certainty in parent body affinity based on texture.

Atmospheric entry parameters, including entry angle and velocity, directly control the peak temperature suffered by CSs and, thus, their final texture (Love and Brownlee, 1991). These entry parameters are the direct result the orbi-

Table 2
Relative abundance of precursor materials (i.e. carbonaceous chondritic, ordinary chondritic and unknown) within CSs from the Transantarctic Mountains and the Atacama Desert.

Subtype	Precursor material (%)		
	Carbonaceous[a]	Ordinary[b]	Unknown[c]
Transantarctic mountains			
BO	88	13	0
Cc	13	75	13
Po	0	89	11
V	47	41	12
Atacama			
BO	82	18	0
Cc	14	57	29
Total			
BO	86	14	0
Cc	13	67	20
Po	0	89	11
V	47	41	12

[a] Isotopic groups 1 and 2.
[b] Isotopic group 3.
[c] Isotopic group 4.

tal evolution of asteroidal dust from their parent body in the asteroid belt to 1 AU. Nesvorný et al. (2006) have developed a model showing the orbital evolution of dust produced by collisions in the main asteroid belt, which shows that after particles >500 μm in size start spiraling toward the Sun because of the Poynting-Robertson drag, disturbances by secular resonances at 2 AU efficiently scatter their eccentricity and inclination. It results in important overlaps in the orbital properties of populations of particles originating from different asteroidal parent bodies. Atmospheric entry parameters of all chondritic CSs are, thus, broadly similar (i.e. similar ranges of entry velocities and random entry angles) and cannot explain the distribution of textures among OC and CC-related CSs. Thus, the distinct internal properties of OC and CC precursors (e.g., mineralogy, grain-size and chemical composition) appear to be a critical criterion to explain the parent body control on the textures of CSs.

Fig. 4 shows a compilation of bulk compositions of stony CSs both <500 μm and >500 μm in size. The compositional fields for subtypes BO, Cc and Po for both normal-sized and large CSs appear to overlap significantly. Only V-type CSs exhibit bulk compositions that are poorer in Fe with respect to other subtypes. This is mainly due to the loss of Fe by evaporation during atmospheric entry heating (Alexander et al., 2002). Furthermore, Fig. 4 shows the parentage (i.e. ordinary of carbonaceous chondrites) of CSs based on their oxygen isotopic signature when this datum was available in the literature (Cordier et al., 2011a; Yada et al., 2005; Suavet et al., 2011; Rudraswami et al., 2015). Note that for ion probe data, only CSs exhibiting unambiguous parentage were included (i.e. taking into account the uncertainties when determining whether the particles plot below or above the TFL; see Section 4.1). It appears that both CC and OC-related CSs show a wide range of bulk composition, which are for both parentages
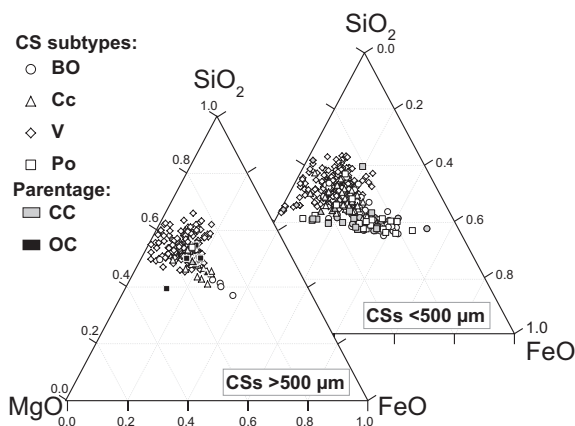
Fig. 4. SiO$_2$-MgO-FeO ternary diagrams showing the bulk compositions of stony cosmic spherules of known subtypes from the literature (Cordier et al., 2011a, 2011b; Yada et al., 2005; Suavet et al., 2011). When known, the CC or OC parentage of the cosmic spherules is indicated.

and for all CSs subtypes similar. Assuming that the compositions of CSs of same subtypes evolve in a similar manner during atmospheric entry, their differences in bulk compositions will reflect their precursor materials. As a result, it appears that the bulk composition of the precursor materials of BO, Cc and Po CSs significantly overlap, thus suggesting that they are not a critical factor controlling the textures of CSs.

Chondrules are good analogs to CSs in terms of mineralogy, texture (i.e., porphyritic and barred olivine are the most common textures observed in chondrules; Brearley and Jones, 1998) and bulk compositions. Given their similar mineralogy and texture, the formation mechanisms of chondrules, which have been extensively studied, may provide constraints on the textures of CSs. Experiments on chondrule formation have shown that in order to produce the porphyritic olivine texture, the survival of nuclei during melting of the precursor material is necessary (Connolly et al., 1998; Hewins et al., 2005). Porphyritic textures in experimentally produced chondrules can form from both fine and coarse-grained precursors at sub-liquidus peak temperatures where cooling rates are sufficiently slow to allow growth of phenocrysts (minutes to hours; Hewins et al., 2005 and references therein). Although the ranges of peak temperatures during the formation of both chondrules and CSs are broadly similar (~1000–1900 °C), the heating pulse is much shorter in CSs (Love and Brownlee, 1991; Hewins et al., 2005). This allows nuclei to survive over a wider range of peak temperatures in CSs, however, the opportunity for crystal growth is significantly restricted by the equally fast cooling rate (in seconds for CSs compared to minutes to hours for chondrules; Love and Brownlee, 1991). Entirely fine-grained precursors are, thus, unlikely to produce sufficiently large nuclei to form the Po texture in CSs. Under conditions of rapid cooling observed in CSs, mainly coarse-grained precursors may, therefore, provide nuclei that are larger than the critical radius necessary to grow phenocrysts. The observation that many Po CSs have phenocrysts containing relict grains several

microns in size (e.g. Genge et al., 2008) supports their formation largely from coarse-grained precursors. Chondrule experiments by Connolly et al. (1998) suggest that a critical factor in producing large euhedral olivine crystals is the number of nuclei surviving after melting of the precursor. A small number of nuclei will grow euhedral olivine crystals more readily owing to minimal competition for components by other crystals. If each precursor crystal leaves a single nucleus after melting, then coarse-grained precursors are more likely to produce optimal nuclei abundances for olivine growth. Conversely, a high number of small nuclei from a fine-grained precursor will increase the competition to form new crystals, resulting in smaller but more numerous subhedral olivine crystals, forming a micro-porphyritic texture that is observed in both chondrules and, CSs (Fig. 5).

Although grain-size is important in the survival of crystal nuclei during melting and the number of crystals that grow on cooling, the chemical composition of the mineral phases constituting the CSs is also an important factor due to its control on the solidus and liquidus temperatures. Coarse-grained precursors made of mineral phases having a wide range of compositions will partially melt over a similarly wide range of peak temperature. This condition will favor the preservation of relicts and, thus, the formation of Po textures. Conversely, if the precursor is made of mineral phases having similar compositions, it will be more likely to melt quickly over a small range of peak temperatures. The only exception is if the precursors' crystals are large enough to partially survive melting and leave relicts that will favor the production of porphyritic textures (Connolly et al., 1998). In contrast, for the reasons mentioned above, under fast cooling rates and independently of the composition of precursor's phases, a fine-grained precursor is less likely to produce nuclei large enough to form porphyritic textures. Barred olivine textures may be formed under such conditions, where a limited number of submicron nuclei are left after melting. However, coarse-grained precursors having a small range of mineral compositions, such as equilibrated ordinary chondrites, that completely melt over a small range of temperature, may also form barred olivine textures, if submicron nuclei are still present.

It is suggested above that Po CSs are likely to form from coarse-grained precursors only, therefore, fine-grained matrices of both unequilibrated ordinary chondrites and carbonaceous chondrites cannot form the Po texture. As a consequence, within chondrites, coarse-grained precursors are likely to be complete or fragments of chondrules. Chondrules are present in both ordinary and carbonaceous chondrites (Brearley and Jones, 1998). The large relict phases observed in Po CSs are, thus, likely to be remains of phases within chondrules (Genge et al., 2008). Based on major and minor element compositions of relict olivine crystals in 19 Po spherules (200–800 μm in size), Cordier et al. (2011b) have shown that ~95% were related to chondrules of either unequilibrated ordinary chondrites or to carbonaceous chondrites and ~5% to chondrules of equilibrated ordinary chondrites. The large abundance of relict olivine crystals in Po CSs showing affinities with chondrules of unequilibrated ordinary and carbonaceous chondrites is
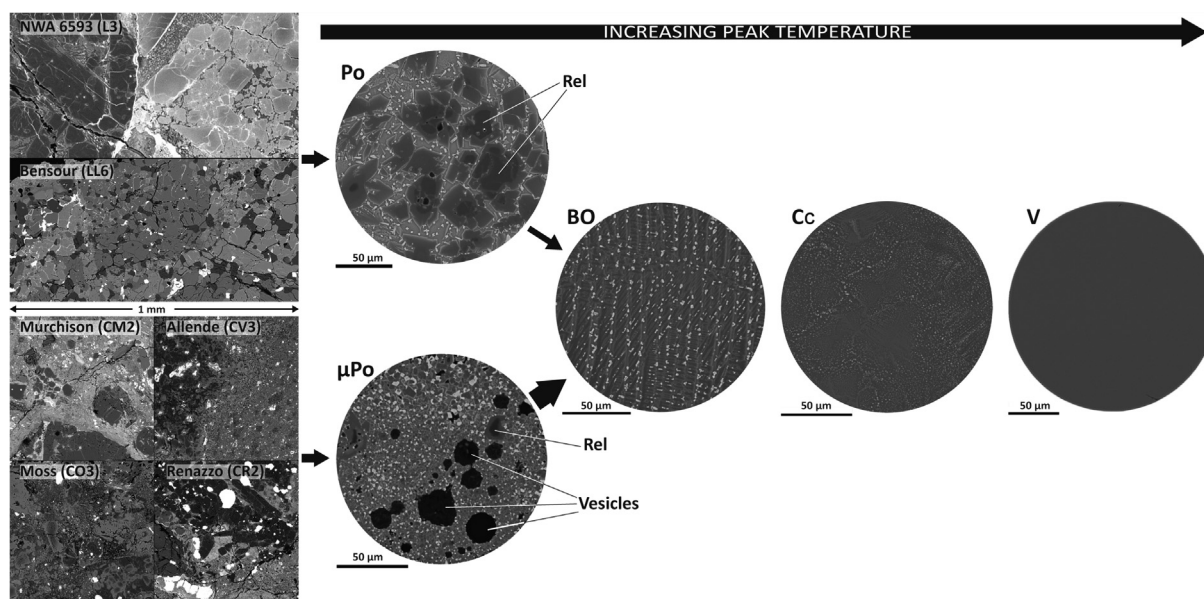
Fig. 5. Backscatter electron images showing the textures of precursors and of the resulting CSs, organized by increasing peak temperature. Coarse-grained ordinary chondritic precursors are illustrated by NWA 6593 (L3) and Bensour (LL6). Mainly fine-grained matrix-rich carbonaceous chondritic precursors are illustrated by Murchison (CM2), Allende (CV3), Moss (CO3) and Renazzo (CR2). Abbreviation: Rel = relict.

likely due to the high melting temperatures of their constituent Mg-rich phases (melting temperatures for enstatite 1557 °C, fayalite 1205 °C, compared to forsterite 1890 °C, Deer et al., 1966). In contrast, equilibrated ordinary chondrites are dominated by Fe-rich olivine and Low-Ca pyroxene (i.e., $\sim Fa_{16}$ to $\sim Fa_{32}$ in olivine of H, L and LL chondrites; Brearley and Jones, 1998), significantly lowering the solidus temperatures of potential CS precursors and the temperature interval over which melting occurs. Spherules with Po textures may still, however, be generated from equilibrated compositions due to the larger size of the olivine crystals in equilibrated ordinary chondrites, which does not have time to melt entirely (Connolly et al., 1998).

That Po CSs >500 μm in size show unambiguous affinities to ordinary chondrites based on their oxygen isotopes may be explained by several factors. Firstly, more than 95% of the chondrules of carbonaceous chondrites, except for CO chondrites, are type I chondrules containing Fe-poor silicates (e.g., $Fa_{\ll 10}$ in olivine; Brearley and Jones, 1998). Consequently the melting temperatures of phenocrysts within these chondrules are both high and span a restricted range of temperatures (e.g., the melting temperature difference between Fa_4 and Fa_0 is only ~ 50 °C). The high melting temperature of the phenocryst phases within Type I chondrules (i.e. ~ 1850 °C) will result in the formation of partially melted coarse-grained micrometeorites over a wide range of peak temperatures with composite micrometeorites, which consist of coarse-grained cores surrounded by an igneous rim, forming where attached fine-grained matrix was present in the precursor particle (Genge, 2006). The range of melting temperatures of Mg-rich phenocrysts furthermore reduces the opportunity for survival of nuclei by restricting the temperature range over which they survive. It suggests that when such precursors of

large CSs are superheated during atmospheric entry (i.e., above the liquidus of nearly pure forsterite), a scenario that is more likely more frequent than for smaller CSs, they will completely melt and quickly lose all nuclei. Subsequent rapid cooling (i.e. few seconds) will favor the formation of V-type CSs.

Precursors that represent fragments of type-II chondrules from carbonaceous chondrites, in contrast, have a wider range of Fe content (e.g., olivine composition ranging from $\sim Fa_0$ to $\sim Fa_{60}$; Brearley and Jones, 1998), meaning that they will start melting over a wider-range of temperatures and that melting initiates at lower peak temperature, and can, therefore, potentially form Po CSs due to enhanced potential for nuclei survival. Type II chondrules are present in only low abundances in all carbonaceous chondrites except CO chondrites. The mean size of chondrules in CO chondrites, however, is small (~ 150 μm) compared to other classes and is much smaller than the size of precursors of large CSs (~ 750 μm, assuming that it is 1.5–2.0 times larger than the resulting CS; Love and Brownlee, 1991). This may explain why Po CSs related to carbonaceous chondrites are observed in smaller size fraction (Yada et al., 2005; Cordier et al., 2011b; Rudraswami et al., 2015) and not among large CSs. Therefore, CO chondrite-related precursors of CSs would contain abundant fine-grained matrix. Although we cannot exclude the formation of Po spherules from chondrules of CO chondrites of relict olivine crystals as nucleation sites to produce Po CSs, we suggest that the probability is low ensuring such spherules are rare in larger size ranges (i.e. >500 μm).

We mentioned earlier the existence of micro-porphyritic textures among Stony CSs, which are commonly classified as simple Po CSs (e.g., Cordier et al., 2011b; Rudraswami et al., 2015). From now on, we will make the distinction

between normal Po CSs, consisting mainly of euhedral crystals of olivine, and micro-porphyritic CSs (hereafter μPo CS), which consist of numerous subhedral olivine crystals, typically ≤10 μm in size, along with frequent vesicles due to the degassing of volatiles during atmospheric entry heating and frequent relict minerals.

Porphyritic and micro-porphyritic textures similar to those of Po and μPo CSs, respectively, are also observed in the outermost layers of the fusion crusts of chondritic meteorites, which suffered complete melting during atmospheric entry (Fig. 6). In contrast, barred olivine textures

Fig. 6. Backscattered electron images of fusion crusts of chondritic meteorites (A) Cold Bokkeveld (CM2), (B) Moss (CO3), (C) Allende (CV3), (D) Allessandria (H5), (E) Assisi (H5) and (F) Borkut (L5). The dashed lines delimits the totally melted outer layer and the substrate of the fusion crusts (Genge and Grady, 1999). The totally melted outer layer of the fusion crusts of carbonaceous chondrites exhibit textures similar to Cc CSs evolving into μPo CSs toward to outer edge, whereas the fusion crusts of ordinary chondrites exhibit textures similar to Po CS. Abbreviation: Rel = relict.

commonly observed in CSs are rarely observed in fusion crusts of meteorites, mainly because of the rapid cooling of CSs compared to fusion crusts, favoring the growth of subhedral to euhedral crystals (Genge and Grady, 1999). The fusion crusts of carbonaceous chondrites tend to exhibit porphyritic textures along the more evolved outer edge, with poorly crystallized magnetite (e.g., in the CM chondrite Alais, the CV chondrite Allende and the CO chondrite Moss in Fig. 7a, b and c, respectively). The textures of the less evolved inner part of these melted crusts are similar to those of μPo, which is consistent with the survival of a large number of nucleation sites due to wide ranges of melting temperature of the mineral phases constituting the matrices of carbonaceous chondrites. The fusion crusts of equilibrated ordinary chondrites, on the other hand, exhibit coarser-grained euhedral olivine crystals with rather constant grain-size throughout, and dendritic magnetic crystals (e.g., the H5 Alessandria, H5 Assisi and L5 Borkut in Fig. 7d, e and f, respectively). These textures are similar to those of Po CSs. These observations on fusion crusts support an ordinary chondritic origin for Po CSs and a carbonaceous chondritic origin for μPo CSs.

Fig. 7 shows that, based on dynamical models of atmospheric entry of micrometeorites (Genge, 2012), the range of atmospheric entry angles under which peak temperatures allow the formation of μPo textures decreases significantly with increasing size of CSs. Thus, most matrix-rich carbonaceous chondritic precursors of large CSs (>500 μm) will be subjected to supercooling, favoring the formation of BO CSs over μPo CSs. As a result, μPo CSs are likely to be rare among large CSs, thus explaining their absence in studies of oxygen isotopic composition using the IRMS techniques (this study; Suavet et al., 2010, 2011). A high-precision oxygen isotope study of CSs from smaller size fraction (<500 μm) is, thus, necessary to confirm the carbonaceous chondritic nature of the precursors of μPo CSs. Finally, it is important to distinguish μPo CSs from Po CSs (i.e. made of large euhedral crystals of olivine). For example, Cordier et al. (2011b) and Rudraswami et al. (2015) studied CC-related CSs <500 μm in size exhibiting both μPo and Po textures, without clearly distinguishing between the two. Making this distinction in future studies may help understanding whether the μPo texture is related to the matrix of CCs rather than to chondrules, and vice versa for the Po texture. As a result of these observations, we propose the addition of the new μPo CS subtype in the micrometeorite classification scheme developed by Genge et al. (2008).

The observation that approximately 67% Cc CSs in both collections are related to ordinary chondrite parent bodies suggests that under supra-liquidus regimes, the number of nuclei after melting of a coarse-grained precursor are not sufficient to produce BO textures. This may explains why Cc CSs are twice as frequent as BO CSs in OC-derived CSs, whereas they are rare among CC-derived CSs (i.e. 1 Cc CS for 30 BO CSs). Conversely, V-type spherules are evenly divided between OC and CC-related CSs. They probably form at the highest peak temperature during entry heating due to destruction of all nuclei followed by rapid cooling. Note that Cc CS #10.17 may be related to EC
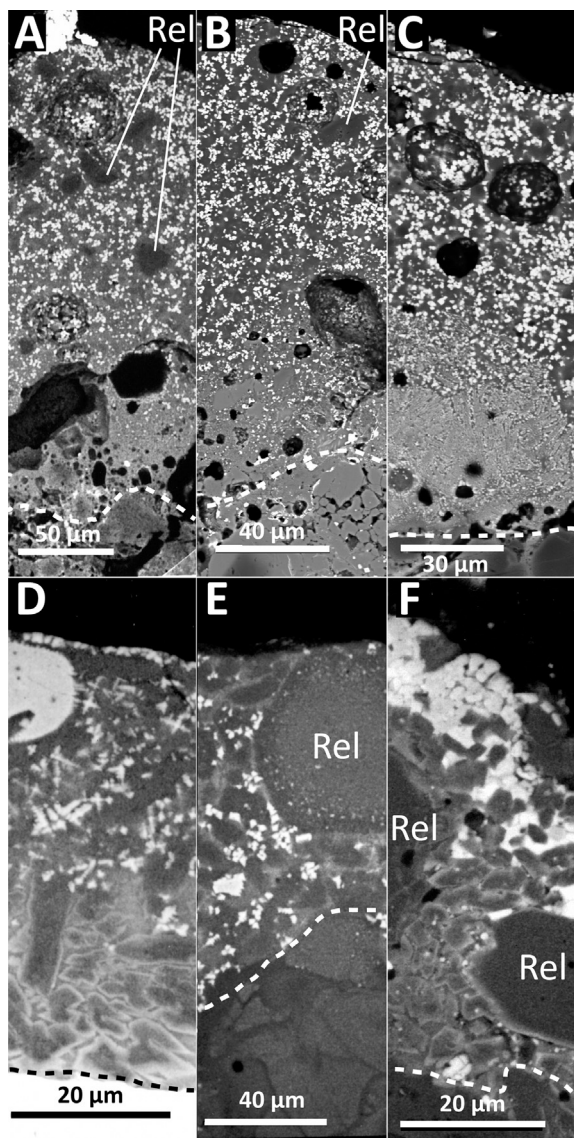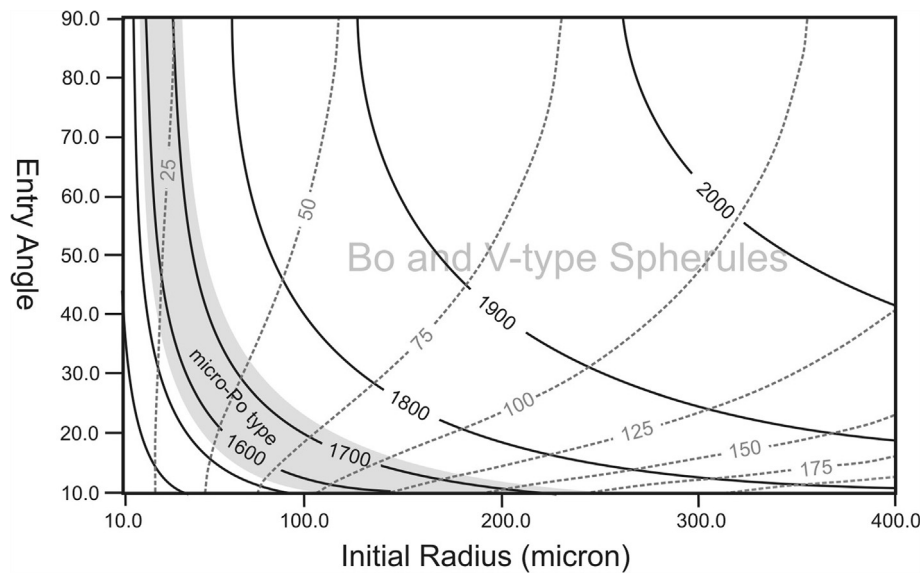
Fig. 7. Entry heating model for a CM2 composition micrometeorite entering the atmosphere at 12 km s^{-1} (Genge, 2012). An example peak temperature interval for the formation of µPo CSs of 1550–1750 K is shown with Bo and V-type spherules forming at higher temperatures. Solid lines show peak temperature attained during deceleration, dashed gray lines show the final radii of CSs after evaporation. The abundance of spherules of a particular size can be approximated by tracing along contours of constant final radii. The abundance of µPo CSs becomes very small compared to those of Bo and V-type spherules with increasing final radii. This diagrams illustrates the maximum abundance of µPo CSs since evaporation increases at higher entry velocities.

material. But ECs exhibit Fe-poor silicate compared to OCs, the grain-size is similar in both materials. As mentioned before for type I chondrules, Fe-poor material may restrict the ranges of temperature for partial melting of coarse-grained material. Therefore, a scenario involving the survival of a sufficient number of nuclei for the formation of Cc texture seems unlikely, and the formation of either unmelted or V-type spherules favored.

The large abundance of the BO texture compared to any other textures for carbonaceous chondrite-related CSs may be explained by the lack of µPo CSs in large size fractions coupled with the heterogeneous nature of the matrices of carbonaceous chondrites. If Type I chondrules from carbonaceous chondrites are unlikely to form Po CSs, this suggests that precursors of carbonaceous chondrite-related CSs are likely to be mainly fragments of fine-grained matrices. The production of the BO texture suggests that at least some nuclei survived melting, as total destruction of all nuclei would result in the production of V-type CSs.

Experiments using matrices of carbonaceous chondrites to form micrometeorites analogs have shown that they melt at relatively low temperature (~1350 °C for CM chondrite material; Toppani et al., 2001). However, some accessory mineral phases of these matrices start melting at much higher temperature (~1600 °C for pure magnetite, which is present in matrices of all carbonaceous chondrites; Zolensky et al., 1993). Even though the grain size of such phases is usually small (< 1 µm), some crystals will likely survive melting to form nuclei. Connolly et al. (1998) have shown that in chondrules, only few nuclei are necessary to form barred olivine textures.

Another factor contributing to the prevalence of the BO texture for CC-related CSs is the presence of metal beads

resulting from the immiscibility of Fe-Ni metal and the silicate melt during atmospheric entry (Genge and Grady, 1998). Metal bead-bearing CSs are thought to be mainly related to carbonaceous chondritic material (Rudraswami et al., 2014). In many metal bead-bearing BO CSs, the orientation of the bars of olivine converge toward metal bead. This suggests that, at least in some cases, metal beads may induce crystallization. As mentioned earlier, the liquidus of the matrices of carbonaceous chondrites is likely lower than the peak temperature suffered during atmospheric entry. Coupled with the fine-grained nature of this material, it quickly leads to complete melting of the precursor, followed in some cases by the formation of liquid metal beads. Although the freezing temperature of the beads depends on its composition, it is likely lower than the freezing point of the silicate melt. Experiments have shown that solid particles can induce crystallization in supercooled silicate melts (Müller et al., 2000). Therefore, it is likely that when a metal bead solidifies in contact with the supercooled silicate melt, nearly instantaneous crystallization of bars of olivine occurs. The presence of V-type spherules related to carbonaceous chondrites show that in some cases complete melting is possible, although marginal. This is probably due to the absence of accessory phases having high melting temperature.

5. CONCLUSION

The oxygen isotopic signatures of cosmic spherules from the Atacama Desert, Chile, are consistent with those from the Transantarctic Mountains (Cordier et al., 2011a; Suavet et al., 2010, 2011), suggesting a distribution of micrometeorite precursors that is global and not biased by abnormal local events. The discovery of a ^{16}O-poor cos-

mic spherules related to the isotopic Group 4 defined by Suavet et al. (2010) confirms that unknown parent bodies contribute significantly to the flux of micrometeorites to Earth.

The texture of the cosmic spherules is mainly controlled by the grain-size and mineralogy of the precursor material. Po cosmic spherules mainly form from coarse-grained precursors mostly having ordinary chondrite compositions. For this precursor material, increasing peak temperatures will favor the formation of cryptocrystalline textures instead of BO textures, due to insufficient number of nuclei. Type I chondrules of carbonaceous chondrites are unlikely to form Po cosmic spherules and will survive atmospheric entry heating or generate V-type CSs at high peak temperatures. Most BO cosmic spherules are related to the matrices of carbonaceous chondrites due to the wide range of melting temperatures of their mineral phases, favoring supercooling. Accessory phases may form sparse nuclei necessary for the crystallization of bars of olivine. The textures of cosmic spherules provide an easy and efficient mean to identify their parent bodies that is accurate to within $\pm 20\%$.

ACKNOWLEDGMENT

REFERENCES

Alexander C. M. O., Taylor S., Delaney J. S., Ma P and Herzog G. F. (2002) Mass-dependent fractionation of Mg, Si, and Fe isotopes in five stony cosmic spherules. *Geochim. Cosmochim. Acta* **66**, 173–183. http://dx.doi.org/10.1016/S0016-7037(01)00764-5.

Alexandre A., Sonzogni C., Basile I., Sylvestre F., Parron C., Meunier J. D. and Colin F. (2006) Oxygen isotope analyses of fine silica grains using laser-extraction technique: comparison with oxygen isotope data obtained from ion microprobe analyses and application to quartzite and silcrete cement investigation. *Geochim. Cosmochim. Acta* **70**, 2827–2835. http://dx.doi.org/10.1016/j.gca.2006.03.003.

Bland P. A., Zolensky M. E., Benedix G. K. and Sephton M. A. (2006) Weathering of chondritic meteorites. *Meteorites Early Sol. Syst. II.*, 853–867.

Brearley A. J. and Jones R. H. (1998) Chondritic meteorites. In *Planetary Materials*, vol. 36 (ed. J. Papike), pp. 1–398. Reviews in Mineralogy (Chapter 3).

Bridges J. C., Franchi I. A., Hutchinson R., Sexton A. S. and Pillinger C. T. (1998) Correlated mineralogy, chemical compositions, oxygen isotopic compositions and size of chondrules. *Earth Planet. Sci.* **155**, 183–196. http://dx.doi.org/10.1016/S0012-821X(97)00213-6.

Chaussidon M., Libourel G. and Krot A. N. (2008) Oxygen isotopic constraints on the origin of magnesian chondrules and on the gaseous reservoirs in the early Solar System. *Geochim. Cosmochim. Acta* **72**, 1924–1938. http://dx.doi.org/10.1016/j.gca.2008.01.015.

Choi B. G., McKeegan K. D., Krot A. N. and Wasson J. T. (1998) Extreme oxygen-isotopic composition in magnetite from unequilibrated ordinary chondrites. *Nature* **392**, 577–579. http://dx.doi.org/10.1038/33356.

Clayton R. N. and Mayeda T. K. (1999) Oxygen isotope studies of carbonaceous chondrites. *Geochim. Cosmochim. Acta* **63**, 2089–2104. http://dx.doi.org/10.1016/S0016-7037(99)00090-3.

Clayton R. N., Mayeda T. K., Olsen E. J. and Goswami J. N. (1991) Oxygen isotope studies of ordinary chondrites. *Geochim. Cosmochim. Acta* **55**, 2317–2337. http://dx.doi.org/10.1016/0016-7037(91)90107-G.

Connolly H. C., Jones B. D. and Hewins R. H. (1998) The flash melting of chondrules: an experimental investigation into the melting history and physical nature of chondrule precursors. *Geochim. Cosmochim. Acta* **62**, 2725–2735. http://dx.doi.org/10.1016/S0016-7037(98)00176-8.

Cordier C. and Folco L. (2014) Oxygen isotopes in cosmic spherules and the composition of the near Earth interplanetary dust complex. *Geochim. Cosmochim. Acta* **146**, 18–26. http://dx.doi.org/10.1016/j.gca.2014.09.038.

Cordier C., Folco L., Suavet C., Sonzogni C. and Rochette P. (2011a) Major, trace element and oxygen isotope study of glass cosmic spherules of chondritic composition: the record of their source material and atmospheric entry heating. *Geochim. Cosmochim. Acta* **75**, 5203–5218. http://dx.doi.org/10.1016/j.gca.2011.06.014.

Cordier C., Van Ginneken M. and Folco L. (2011b) Nickel abundance in stony cosmic spherules: constraining precursor material and formation mechanisms. *Meteorit. Planet. Sci.* **46**, 1110–1132. http://dx.doi.org/10.1111/j.1945-5100.2011.01218.x.

Cordier C., Suavet C., Folco L., Rochette P. and Sonzogni C. (2012) HED-like cosmic spherules from the Transantarctic Mountains, Antarctica: major and trace element abundances and oxygen isotopic compositions. *Geochim. Cosmochim. Acta* **77**, 515–529. http://dx.doi.org/10.1016/j.gca.2011.10.021.

Crespin J., Alexandre A., Sylvestre F., Sonzogni C., Paillès C. and Garreta V. (2008) IR laser extraction technique applied to oxygen isotope analysis of small biogenic silica samples. *Anal. Chem.* **80**, 2372–2378. http://dx.doi.org/10.1021/ac071475c.

Day R. (1977) Hysteresis properties of titanomagnetites: grain-size and compositional dependance. *Phys. Earth Planet. Inter.* **13**, 260–267. http://dx.doi.org/10.1016/0031-9201(77)90108-X.

Deer W. A., Howie R. A. and Zussman J. (1966) *Introduction to the Rock-Forming Minerals.* Wiley, New York.

De Leuw S., Rubin A. E. and Wasson J. T. (2010) Carbonates in CM chondrites: complex formational histories and comparison to carbonates in CI chondrites. *Meteorit. Planet. Sci.* **45**, 513–530. http://dx.doi.org/10.1111/j.1945-5100.2010.01037.x.

Dunlop D. J. (2002) Theory and application of the Day plot (Mrs/Ms vs. Hcr/Hc). 1. Theoretical curves and tests using titano-magnetite data. *J. Geophys. Res.* **107**, B3. http://dx.doi.org/10.1029/2001JB000486.

Endreß M. and Bischoff A. (1996) Carbonates in CI chondrites: clues to parent body evolution. *Geochim. Cosmochim. Acta* **60**, 489–507.

Engrand C. and Maurette M. (1998) Carbonaceous micrometeorites from Antarctica. *Meteorit. Planet. Sci.* **33**, 565–580. http://dx.doi.org/10.1111/j.1945-5100.1998.tb01665.x.

Engrand C., McKeegan K. D., Leshin L. A., Herzog G. F., Schnabel C., Nyquist L. E. and Brownlee D. E. (2005) Isotopic

compositions of oxygen, iron, chromium, and nickel in cosmic spherules: toward a better comprehension of atmospheric entry heating effects. *Geochim. Cosmochim. Acta* **69**, 5365–5385. http://dx.doi.org/10.1016/j.gca.2005.07.002.

Flynn G. J., Durda D. D., Minnick M. A. and Strait M. (2009) Production of cosmic dust by hydrous and anhydrous asteroids: implications for the production of interplanetary dust particles and micrometeorites. In *40th Lunar and Planetary Science Conference, abstract #1164*.

Franchi I. A., Wright I. P., Sexton A. S. and Pillinger C. T. (1999) The oxygen-isotopic composition of Earth and Mars. *Meteorit. Planet. Sci.* **34**, 657–661. http://dx.doi.org/10.1111/j.1945-5100.1999.tb01371.x.

Genge M. J. (2006) Igneous rims on micrometeorites. *Geochim. Cosmochim. Acta* **70**, 2603–2621. http://dx.doi.org/10.1016/j.gca.2006.02.005.

Genge M. J. (2008) Koronis asteroid dust within Antarctic ice. *Geology* **36**, 687–690. http://dx.doi.org/10.1130/G24493A.1.

Genge M. J. (2012) The atmospheric entry and abundance of basaltic micrometeorites. In *75th Ann. Meet. of Met. Soc., Abstract #5078, A-145*.

Genge M. J. and Grady M. M. (1998) Melted micrometeorites from Antarctic ice with evidence for the separation of immiscible Fe–Ni–S liquids during entry heating. *Meteorit. Planet. Sci.* **33**, 425–434.

Genge M. J. and Grady M. M. (1999) The fusion crusts of stony meteorites: implications for the atmospheric reprocessing of extraterrestrial materials. *Meteorit. Planet. Sci.* **34**, 341–356. http://dx.doi.org/10.1111/j.1945-5100.1999.tb01344.x.

Genge M. J., Engrand C., Gounelle M. and Taylor S. (2008) The classification of micrometeorites. *Meteorit. Planet. Sci.* **43**, 497–515. http://dx.doi.org/10.1111/j.1945-5100.2008.tb00668.x.

Hewins R. H., Connolly H. C., Lofgren G. E. and Libourel G. (2005) Experimental constraints on chondrule formation. In *Chondrites and the Protoplanetary Disk. ASP Conference Series*, vol. 341, pp. 286–316. Chondrites and the Protoplanetary Disk. ASP Conference Series.

Hezel D., Russell S., Ross A. J. and Kearsley A. T. (2008) Modal abundances of CAIs: implications for bulk chondrite element abundances and fractionations. *Meteorit. Planet. Sci.* **43**, 1879–1894. http://dx.doi.org/10.1111/j.1945-5100.2008.tb00649.x.

Howard K. T., Benedix G. K., Bland P. A. and Cressey G. (2009) Modal mineralogy of CM2 chondrites by X-ray diffraction (PSD-XRD). Part 1: Total phyllosilicate abundance and the degree of aqueous alteration. *Geochim. Cosmochim. Acta* **73**, 4576–4589. http://dx.doi.org/10.1016/j.gca.2009.04.038.

Hutzler A., Gattacceca J., Rochette P., Braucher R., Carro B., Christensen E. J., Cournede C., Gounelle M., Laridhi Ouazaa N., Martinez R., Valenzuela M., Warner M. and Bourlès D. (2016) Description of a very dense meteorite collection area in western Atacama: insight into the long-term composition of the meteorite flux to Earth. *Meteorit. Planet. Sci.* **51**, 468–482. http://dx.doi.org/10.1111/maps.12607.

King A. J., Schofield P. F., Howard K. T. and Russell S. R. (2015) Modal mineralogy of CI and CI-like chondrites by X-ray diffraction. *Geochim. Cosmochim. Acta* **165**, 148–160. http://dx.doi.org/10.1016/j.gca.2015.05.038.

Kohout T., Kallonen A., Suuronen J. P., Rochette P., Hutzler A., Gattacceca J., Badjukov D. D., Skála R., Böhmová V. and Čuda J. (2014) Density, porosity, mineralogy, and internal structure of cosmic dust and alteration of its properties during high-velocity atmospheric entry. *Meteorit. Planet. Sci.* **49**, 1157–1170. http://dx.doi.org/10.1111/maps.12325.

Libourel G. and Chaussidon M. (2011) Oxygen isotopic constraints on the origin of Mg-rich olivines from chondritic meteorites. *Earth Planet. Sci. Lett.* **301**, 9–21. http://dx.doi.org/10.1016/j.epsl.2010.11.009.

Love S. G. and Brownlee D. E. (1991) Heating and thermal transformation of micrometeoroids entering the Earth's atmosphere. *Icarus* **89**, 26–43. http://dx.doi.org/10.1016/0019-1035(91)90085-8.

Müller R., Zanotto E. D. and Fokin V. M. (2000) Surface crystallization of silicate glasses: nucleation sites and kinetics. *J. Non-Cryst. Solids* **274**, 208–231.

Nesvorný D., Vokrouhlický D., Bottke W. F. and Sykes M. (2006) Physical properties of asteroid dust bands and their sources. *Icarus* **181**, 107–144. http://dx.doi.org/10.1016/j.icarus.2005.10.022.

Newton J., Franchi I. A. and Pillinger C. T. (2000) The oxygen isotopic record in enstatite meteorites. *Meteorit. Planet. Sci.* **35**, 689–698. http://dx.doi.org/10.1111/j.1945-5100.2000.tb01452.x.

Noguchi T., Nakamura T. and Nozaki N. (2002) Mineralogy of phyllosilicate-rich micrometeorites and comparison with Tagish Lake and Sayama meteorites. *Earth Planet. Sci. Lett.* **202**, 229–246. http://dx.doi.org/10.1016/S0012-821X(02)00777-X.

Rochette P., Folco L., Suavet C., Van Ginneken M., Gattacceca J., Perchiazzi N., Braucher R. and Harvey R. P. (2008) Micrometeorites from the Transantarctic Mountains. *Proc. Natl. Acad. Sci. USA* **47**, 18206–18211. http://dx.doi.org/10.1073/pnas.0806049105.

Rubin A. E. and Grossman J. N. (2010) Meteorite and meteoroid: new comprehensive definitions. *Meteorit. Planet. Sci.* **45**, 114–122. http://dx.doi.org/10.1111/j.1945-5100.2009.01009.x.

Rudraswami N. G., Ushikubo T., Nakashima D. and Kita N. T. (2011) Oxygen isotope systematics of chondrules in the Allende CV3 chondrite: high precision ion microprobe studies. *Geochim. Cosmochim. Acta* **75**, 7596–7611. http://dx.doi.org/10.1016/j.gca.2011.09.035.

Rudraswami N. G., Shyam Prasad M., Babu E. V. S. S. K. and Vijaya Kumar M. (2014) Chemistry and petrology of Fe–Ni beads from different types of cosmic spherules: implication for precursors. *Geochim. Cosmochim. Acta* **145**, 139–158. http://dx.doi.org/10.1016/j.gca.2014.09.029.

Rudraswami N. G., Shyam Prasad M., Nagashima K. and Jones R. H. (2015) Oxygen isotopic composition of relict olivine grains in cosmic spherules: links to chondrules from carbonaceous chondrites. *Geochim. Cosmochim. Acta* **164**, 53–70. http://dx.doi.org/10.1016/j.gca.2015.05.004.

Sakamoto N., Seto Y., Itoh S., Kuramoto K., Fujino K., Nagashima K., Krot A. N. and Yurimoto H. (2007) Remnants of the early solar system water enriched in heavy oxygen isotopes. *Science* **317**, 231–233. http://dx.doi.org/10.1126/science.1142021.

Suavet C., Gattacceca J., Rochette P., Perchiazzi N., Folco L., Duprat J. and Harvey R. P. (2009) Magnetic properties of micrometeorites. *J. Geophys. Res.* **114**, B04102. http://dx.doi.org/10.1029/2008JB005831.

Suavet C., Alexandre A., Franchi I. A., Gattacceca J., Sonzogni C., Greenwood R. C., Folco L. and Rochette P. (2010) Identification of the parent bodies of micrometeorites with high-precision oxygen isotope ratios. *Earth Planet. Sci. Lett.* **293**, 313–320. http://dx.doi.org/10.1016/j.epsl.2010.02.046.

Suavet C., Cordier C., Rochette P., Folco L., Gattacceca J., Sonzogni C. and Damphoffer D. (2011) Ordinary chondrite-related giant (>800 7μm) cosmic spherules from the Transantarctic Mountains, Antarctica. *Geochim. Cosmochim. Acta* **75**, 6200–6210. http://dx.doi.org/10.1016/j.gca.2011.07.034.

Taylor S., Lever J. H. and Harvey R. P. (1998) Numbers, types and compositions of an unbiased collection of cosmic spherules. *Meteorit. Planet. Sci.* **35**, 651–666.

Taylor S., Alexander C. M. O'. D., Delaney G., Ma P., Herzog G. F. and Engrand C. (2005) Isotopic fractionation of iron, potassium, and oxygen in stony cosmic spherules: implications for heating histories and sources. *Geochim. Cosmochim. Acta* **69**, 2647–2662. http://dx.doi.org/10.1016/j.gca.2004.11.027.

Taylor S., Matrajt G. and Guan Y. (2012) Fine-grained precursors dominate the micrometeorite flux. *Meteorit. Planet. Sci.* **47**, 550–564. http://dx.doi.org/10.1111/j.1945-5100.2011.01292.x.

Tenner T. J., Ushibuko T., Kurahashi E., Kita N. T. and Nagahara H. (2013) Oxygen isotope systematics of chondrule phenocrysts from the CO3.0 chondrite Yamato 81020: evidence for two distinct oxygen isotope reservoirs. *Geochim. Cosmochim. Acta* **102**, 226–245. http://dx.doi.org/10.1016/j.gca.2012.10.034.

Tenner T. J., Nakashima D., Ushikubo T., Kita N. T. and Weisberg M. K. (2015) Oxygen isotope ratios of FeO-poor chondrules in CR3 chondrites: Influence of dust enrichment and H$_2$O during chondrule formation. *Geochim. Cosmochim. Acta* **148**, 228–250. http://dx.doi.org/10.1016/j.gca.2014.09.025.

Thiemens M., Jackson T., Zipf E., Erdman P. W. and Van Egmond C. (1995) Carbon dioxide and oxygen isotope anomalies in the mesosphere and stratosphere. *Science* **270**, 969–972. http://dx.doi.org/10.1126/science.270.5238.969.

Toppani A., Libourel G., Engrand C. and Maurette M. (2001) Experimental simulation of atmospheric entry of micrometeorites. *Meteorit. Planet. Sci.* **36**, 1377–1396. http://dx.doi.org/10.1111/j.1945-5100.2001.tb01831.x.

Van Ginneken M., Genge M. J., Folco L. and Harvey R. P. (2016) The weathering of micrometeorites from the Transantarctic Mountains. *Geochim. Cosmochim. Acta* **179**, 1–31. http://dx.doi.org/10.1016/j.gca.2015.11.045.

Wakaki S., Itoh S., Tanaka T. and Yurimoto H. (2013) Petrology, trace element abundances and oxygen isotopic compositions of a compound CAI–chondrule object from Allende. *Geochim. Cosmochim. Acta* **102**, 261–279. http://dx.doi.org/10.1016/j.gca.2012.10.039.

Weisberg M. K., Ebel D. S., Connolly, Jr., H. C., Kita N. T. and Ushikubo T. (2011) Petrology and oxygen isotope compositions of chondrules in E3 chondrites. *Geochim. Cosmochim. Acta* **75**, 6556–6569. http://dx.doi.org/10.1016/j.gca.2011.08.040.

Yada T., Nakamura T., Noguchi T., Matsumoto N., Kusakabe M., Hiyagon H., Ushikubo T., Sugiura N., Kojima H. and Takaoka N. (2005) Oxygen isotopic and chemical compositions of cosmic spherules collected from the Antarctic ice sheet: implications for their precursor materials. *Geochim. Cosmochim. Acta* **69**, 5789–5804. http://dx.doi.org/10.1016/j.gca.2005.08.002.

Yu Y., Hewins R. H., Clayton R. N. and Mayeda T. K. (1995) Experimental study of high temperature oxygen isotope exchange during chondrule formation. *Geochim. Cosmochim. Acta* **59**, 2095–2104. http://dx.doi.org/10.1016/0016-7037(95)00129-8.

Zolensky M., Barrett R. and Browning L. (1993) Mineralogy and composition of matrix and chondrule rims in carbonaceous chondrites. *Geochim. Cosmochim. Acta* **57**, 3123–3148. http://dx.doi.org/10.1016/0016-7037(93)90298-B.

Associate editor: Christian Koeberl